



CHORUS

This is the accepted manuscript made available via CHORUS. The article has been published as:

Hubbard model corrections in real-space x-ray spectroscopy theory

Towfiq Ahmed, J. J. Kas, and J. J. Rehr

Phys. Rev. B **85**, 165123 — Published 16 April 2012

DOI: [10.1103/PhysRevB.85.165123](https://doi.org/10.1103/PhysRevB.85.165123)

Hubbard model corrections in real-space x-ray spectroscopy theory

Towfiq Ahmed, J. J. Kas, and J. J. Rehr
Dept. of Physics, Univ. of Washington Seattle, WA 98195
(Dated: March 29, 2012)

The Hubbard model is implemented in real-space multiple scattering (RSMS) Green's function calculations of x-ray spectra based on a rotationally invariant LDA+ U formalism. Values of the Hubbard parameter U are estimated using the constrained RPA method. Our treatment also includes a model self-energy which incorporates the interaction of the photo-electron with excitations such as plasmons; this model is based on an electron gas Green's function and a many-pole model of the screened Coulomb interaction W . This combined treatment leads to an efficient approach to account for correlation on localized as well as delocalized electrons, and the effects on x-ray spectra. Moreover, the RSMS formalism is also applicable to general aperiodic systems including nano-particles, molecules, and surfaces. Results are presented for the spin and angular momentum projected density of states of MnO, NiO, and $\text{La}_{2-x}\text{Sr}_x\text{CuO}_4$ (LSCO), for the K-edge x-ray spectra of O atoms in MnO and NiO, and the unoccupied electronic states and O K-edge spectra of undoped LSCO. The method is found to yield reasonable agreement with experiment.

PACS numbers: 78.70.Dm, 71.10.Fd, 71.10.-w, 71.15.Qe

Keywords: Hubbard model, RSMS, LSCO, GW + U, K-edge XANES

I. INTRODUCTION

Density functional theory (DFT) together with quasi-particle corrections has been remarkably successful in describing the electronic structure and band-gaps of weakly interacting s - p bonded systems. For such systems, quasi-particle corrections are often well described in terms of Hedin's GW self-energy,^{1,2} where G refers to the one-particle Green's function and W the screened Coulomb interaction. Such corrections are especially important in treatments of excited states, e.g., in various x-ray spectra. However, the GW approach is generally inadequate to describe the band gap and other electronic properties in materials with well localized $3d$ or $4f$ electrons.^{3,4} On the other hand, the strong Coulomb interactions in these systems are often approximated using a Hubbard-model,³ in which the on-site electron-electron repulsion is represented by the spin- and orbital-occupancy dependent potential parametrized by "Hubbard parameters" U and J . Combining the local density approximation (LDA) of DFT with the Hubbard model leads to the LDA+ U method. In practice, the Hubbard correction is added to the original Kohn-Sham LDA Hamiltonian while an approximate mean-field term is subtracted to avoid double-counting.⁵ Formally the Hubbard interaction can be regarded as a static approximation to the self-energy of correlated systems.⁶ In calculations of excited state properties, however, one also needs dynamic self-energy effects due to delocalized excitations, i.e., plasmons etc., which can be approximated by model GW calculations. A related approach has been proposed by Jiang *et al.*^{6,7} where a GW self-energy is calculated from an LDA+ U starting point and the infamous double counting terms largely cancel. Their approach also yields good approximations for the band-gap of several d and f electron systems.^{6,7} In another prescription, Bansil *et al.* developed a self-consistent GW+ U scheme based on the tight-binding ap-

proximation and a single-band Hubbard model.^{8,9} Their method is found to qualitatively explain several pre-edge spectral features in high T_c cuprates.^{10,11}

The approach developed here is based on the LDA+ U formalism of Anisimov *et al.*,⁵ together with a many-pole model self-energy, that treats all excitations as plasmonic in nature. This model is not expected to contribute appreciably to the correlation effects on localized states, so we simply add the two contributions to form an effective self-energy correction $\Delta\Sigma^U(E)$. The implementation of our Hubbard-corrected self-energy into the real-space multiple scattering (RSMS) Green's function formalism is relatively straightforward, and yields an efficient approach which is applicable to both weakly and strongly-correlated materials. Our RSMS/ $\Delta\Sigma^U$ approach is advantageous for calculations of x-ray spectra over a broad spectrum, especially since it does not rely on structural symmetry or periodicity requirements.

Using this extension of our RSMS codes, we investigate the effects of correlation on the angular momentum projected density of states (*IDOS*), the x-ray absorption spectra (XAS), and the x-ray emission spectra (XES) of several materials. Other codes which can incorporate Hubbard corrections to excited state spectra include WIEN2K,¹² SPRKKR,¹³ and Quantum ESPRESSO.¹⁴ Our implementation of the Hubbard correction is similar to that in SPRKKR, although in that code U is taken as a parameter.¹³ We also estimate U using the constrained RPA method implemented in our RSMS codes. Calculations of the Hubbard U have also been carried out by others, using both constrained LDA (cLDA¹⁵⁻²⁰), and constrained RPA (cRPA^{21,22}) approaches. Both of these methods have been systematically compared by Aryasetiawan *et al.*²³

Our RSMS/ $\Delta\Sigma^U$ method is tested on several d -electron systems including MnO, NiO, and the undoped high T_c cuprate $\text{La}_{2-x}\text{Sr}_x\text{CuO}_4$ (LSCO). In these mate-

rials, the electronic structure and band gaps are strongly influenced by the Hubbard interaction. We find that our approach yields reasonable agreement with bulk-sensitive probes such as XES and XAS which are used to measure band gaps between occupied and unoccupied states.²⁴ We compare our results with related calculations for MnO and NiO using the GW@LDA+ U treatment of Jiang *et al.*⁶ Treatments of Ti oxide compounds using LDA+ U within the multiple scattering formalism have also been reported by Krüger,²⁵ although, in that work a gap in the d -states was forced by splitting the occupied and unoccupied states by an experimental gap correction.

II. THEORY AND METHODOLOGY

In this section we describe our implementation of the $\Delta\Sigma^U(E)$ method as an extension of the RSMS Green's function formalism.^{26,27} Our implementation generally follows the strategy used in the FEFF9 code, and thus permits calculations of both electronic structure and x-ray spectra that account for atomic correlation effects. Hartree atomic units ($e = \hbar = m = 1$) are implicit unless otherwise specified.

A. RSMS Method

We begin with a brief outline of the RSMS formalism used in this work. In this approach physical quantities of interest are expressed in terms of the quasi-particle Green's function $G(\mathbf{r}, \mathbf{r}', E)$. For example, the physical quantity measured in XAS for photons of polarization $\hat{\epsilon}$ and energy ω is the x-ray absorption coefficient $\mu(\omega)$,

$$\mu(\omega) \propto -\frac{2}{\pi} \text{Im} \langle \phi_c | \hat{\epsilon} \cdot \mathbf{r} G(\mathbf{r}, \mathbf{r}', \omega + E_c) \hat{\epsilon} \cdot \mathbf{r}' | \phi_c \rangle, \quad (1)$$

where E_c is the core electron energy and $|\phi_c\rangle$ is the core state wave function. The FEFF9 code also calculates closely related quantities such as the spin and angular momentum projected density of states (IDOS) $\rho_{l\sigma}^{(n)}(E)$ at site n ,

$$\rho_{l\sigma}^{(n)}(E) = -\frac{1}{\pi} \text{Im} \sum_m \int_0^{R_n} G_{L,L'}^{\sigma,\sigma'}(r, r, E) r^2 dr, \quad (2)$$

where R_n is the Norman radius around the n^{th} atom,²⁸ which is analogous to the Wigner-Seitz radius of neutral spheres. The coefficients $G_{L,L'}^{\sigma,\sigma'}$ characterize the expansion of the Green's function $G(\mathbf{r}, \mathbf{r}', E)$ in spherical harmonics,

$$G(\mathbf{r}, \mathbf{r}', E) = \sum_{L,L',\sigma} Y_L(\hat{\mathbf{r}}) G_{L,L'}^{\sigma,\sigma'}(r, r', E) Y_{L'}^*(\hat{\mathbf{r}}'), \quad (3)$$

where $L = (l, m)$ denotes both orbital and azimuthal quantum numbers. In these formulae, the quasi-particle

Green's function for an excited electron at energy E is given formally (matrix-indices suppressed) by

$$G(E) = [E - H - \Sigma(E)]^{-1}, \quad (4)$$

where H is the Hartree Hamiltonian

$$H = \frac{p^2}{2} + V, \quad (5)$$

and V is the Hartree-potential. For convenience in our calculations, the Hamiltonian is re-expressed in terms of a Kohn-Sham Hamiltonian $H^{KS} = H + V_{xc}$ where V_{xc} is a ground state exchange-correlation²⁹ functional, and the self-energy is replaced by a modified self-energy $\Sigma(E) - V_{xc}$ which is set to zero at the Fermi-energy $E = E_F$. In this work we use the von Barth-Hedin LSDA functional $V_{xc}[n(\mathbf{r}), m(\mathbf{r})]$,²⁹ where $n(\mathbf{r}) = n_\uparrow + n_\downarrow$ is the total electron density and $m(\mathbf{r}) = n_\uparrow - n_\downarrow$ is the spin polarization density. In practice, it is useful to decompose the total Green's function $G(E)$ as

$$G(E) = G^c(E) + G^{sc}(E), \quad (6)$$

where $G^c(E)$ is the contribution from the central (absorbing) atom and $G^{sc}(E)$ is the scattering part. Full multiple scattering (FMS) calculations can be carried out by matrix inversion, i.e., with $G = [1 - G^0 T]^{-1} G^0$, where G^0 is the bare propagator and T is the scattering T -matrix, which are represented in an angular-momentum and site basis: $G^0 = G_{nL,n'L'}^0(E)[1 - \delta_{n,n'}]$ and $T = t_{nL}^\sigma \delta_{L,L'} \delta_{n,n'} \delta_{\sigma,\sigma'}$. Finally, t_{nL}^σ is the single site scattering t -matrix, which is related to partial wave phase shifts,

$$t_{nL}^\sigma = e^{i\delta_{nL}^\sigma} \sin(\delta_{nL}^\sigma). \quad (7)$$

Within the spherical muffin-tin approximation, $G^c(E)$ can be expanded in terms of the regular $R_L(\mathbf{r}, E)$ and irregular $H_L(\mathbf{r}, E)$ solutions of the single site Schrödinger equation.³⁰ In the FEFF code a typical calculation of the electronic structure (ground or excited state) starts with a self-consistent calculation of the electron density and Kohn-Sham potentials.²⁸ Once the self-consistent potential is obtained, the Green's function is constructed and used to calculate XAS and other quantities of interest. Of particular interest in this paper is the spin-dependent density matrix for the n -th site

$$n_{nlm,nlm'}^{\sigma\sigma'} = -\frac{1}{\pi} \int^{E_F} dE \int_{\text{cell}} \text{Im} G_{nlm,nlm'}^{\sigma\sigma'}(\mathbf{r}, \mathbf{r}, E) d^3r, \quad (8)$$

where the n denotes the cell defined by the Norman sphere centered about the n^{th} atom, \mathbf{r}, \mathbf{r}' are relative to the center of the cell R_n , and σ is the spin-index, and we explicitly designate the azimuthal quantum numbers m and m' . For a more detailed description of the multiple scattering RSMS method see Refs. [30,31].

B. GW Many-pole Self-energy

Quasi-particle effects are key to an accurate treatment of excited state spectra,²⁶ and hence require a good approximation for the electron self-energy for extended states. Current approximations for the self-energy typically begin with Hedin's *GW* approximation (GWA),² which is formally given by

$$\Sigma^{GW} = iGW, \quad (9)$$

where G is the one electron Green's function, $W = \epsilon^{-1}v$, is the screened-Coulomb interaction, and v the bare-Coulomb interaction. The FEFF9 code uses several approximations for the self-energy with the aim of providing efficient calculations of the energy dependent shift and broadening of spectral features over a wide energy range. The default, which is appropriate at high energies, is the Hedin-Lundqvist plasmon-pole model,^{2,32} based on the homogeneous electron gas and a single-pole approximation to the dielectric function, which works well at energies above the plasmon energy ω_p . An extension which improves the self energy at lower energies is a many-pole model (MPSE), where the dielectric function is represented as a weighted sum of poles matched to calculations of the loss function in the long wavelength limit.³³ Efficiency is retained by assuming a simple plasmon dispersion relation for all poles in the representation of the dielectric function, and by using an electron gas Green's function. Thus our MPSE calculations are performed in a two step process: (i) The first step is to obtain a suitable approximation to the energy loss function $L(\omega) = -\text{Im}[\epsilon(\mathbf{q} = 0, \omega)^{-1}]$; and (ii) The second is to extend the $q = 0$ result to finite momentum transfer by representing it as a weighted sum of poles, which together conserve the overall oscillator strength,

$$L(q, \omega)^{-1} = -\text{Im}[\epsilon(q, \omega)^{-1}] = \pi \sum_i g_i \omega_i^2 \delta[\omega^2 - \omega_i(q)^2]. \quad (10)$$

Using this representation, and the electron gas approximation for the Green's function, the self-energy is a simple weighted sum of dynamic electron gas plasmon pole self energies, and a Hartree-Fock exchange term

$$\begin{aligned} \Sigma^{MP}(k, E) &= \Sigma_d(k, E) + \Sigma_{HF}(k), \\ \Sigma_d(k, E) &= \sum_i g_i \Sigma_d(k, E; \omega_i). \end{aligned} \quad (11)$$

The above formula is used to calculate an average quasi-particle correction $\Delta\Sigma^{MP}(k(E), E; \rho_{int})$, where the density used in the model is averaged over the interstitial (outside the muffin tins). More details of the MPSE model can be found in Ref. [33].

Although these models significantly improve quasi-particle calculations of unoccupied states at intermediate energies, they do not necessarily yield accurate band-gap corrections, and they do not have an appreciable effect on the localized states near the Fermi energy. Formally

the two effects can be added by assuming that the Hubbard corrections are equivalent to the static Coulomb-hole/screened exchange (COHSEX) approximation for the localized states,⁶ and then treating only the dynamic self-energy corrections to the localized states with the model self-energy, i.e.,

$$\Sigma \approx \Sigma_{\text{COHSEX}} + [\Sigma^{\text{MPSE}} - \Sigma_{\text{COHSEX}}^{\text{MPSE}}]. \quad (12)$$

Here the first term is approximated using the Hubbard model while the second is calculated using our many-pole model. Delocalized states are treated with the many-pole model alone. However, since our many-pole model gives only small quasi-particle corrections to the localized states, we have neglected the last term $\Sigma_{\text{COHSEX}}^{\text{MPSE}}$ in our calculations. Thus in our implementation of the Hubbard corrected self-energy, an effective spin and orbital dependent total correction $\Delta\Sigma^U(E)$ is constructed as a simple addition of the plasmon-pole or many-pole self energy correction $\Delta\Sigma(E)$ and a Hubbard correction V_{lm}^U with calculated U , in order to correct the localized states near the Fermi level. Although such a construction can be done using self-consistent methods,³⁴ here we use only a single-step calculation. Thus we define our total self-energy correction $\Delta\Sigma^U$ as

$$V(\mathbf{r}, E) = V_\sigma^{LDA}(\mathbf{r}) + \Sigma^U(E), \quad (13)$$

$$\Delta\Sigma_{lm\sigma}^U(E) = V_{lm\sigma}^U + \Delta\Sigma^{MP}(E), \quad (14)$$

where each term has double counting subtracted. The orbital and spin-dependent Hubbard contribution to the potential $V_{lm\sigma}^U$ is calculated as described in the next section. We stress that the above prescription is an approximation; formally⁷ one might expect some double-counting between the Hubbard terms and the many-pole self-energy. However, the effect of $\Sigma^{MP}(E)$ is most important at energies comparable to plasmon excitations while the behavior near the band-gaps is dominated by the Hubbard terms.

C. Calculation of U from cRPA

In our cRPA formulation²³ of the Hubbard parameter U we start with the standard expression of the RPA screened Coulomb interaction given by

$$W = \epsilon^{RPA}(\mathbf{r}, \mathbf{r}', \omega)^{-1}v, \quad (15)$$

where the RPA dielectric constant is

$$\epsilon^{RPA}(\mathbf{r}, \mathbf{r}', \omega) = 1 - v\chi^0(\mathbf{r}, \mathbf{r}', \omega). \quad (16)$$

and the non-interacting response function is

$$\begin{aligned} \chi^0(\mathbf{r}, \mathbf{r}', \omega) &= \sum_i^{occ} \sum_j^{unocc} \psi_i(\mathbf{r})\psi_i^*(\mathbf{r}')\psi_j^*(\mathbf{r})\psi_j(\mathbf{r}') \\ &\times \left[\frac{1}{\omega - \epsilon_j + \epsilon_i + i0^+} - \frac{1}{\omega + \epsilon_j - \epsilon_i - i0^+} \right]. \end{aligned} \quad (17)$$

For correlated materials with narrow $3d$ or $4f$ bands, the response function can be divided into $\chi^0 = \chi_d^0 + \chi_r^0$. Here χ_d^0 contains only $3d-3d$ interaction, and can be obtained by limiting the summation to $i, j \in \psi_d$, and χ_r^0 is the response due to the remainder of the states. The effective Coulomb interaction in the narrow $3d$ bands can thus be identified²² with the Hubbard parameter U :

$$U(\mathbf{r}, \mathbf{r}', \omega) = [1 - v\chi_r^0(\mathbf{r}, \mathbf{r}', \omega)]^{-1}v, \quad (18)$$

In the static limit ($\omega = 0$), we retain only the components of the effective interaction on the same atomic site by

$$U = \int_0^{R_n} d^3r d^3r' |\phi_{3d}(\mathbf{r})|^2 U(\mathbf{r}, \mathbf{r}') |\phi_{3d}(\mathbf{r}')|^2, \quad (19)$$

where ϕ_{3d} is the localized $3d$ orbital of the embedded n -th atom with muffin-tin radius R_n . Following Stott and Zaremba,³⁵ we write the $\chi^0(\mathbf{r}, \mathbf{r}', \omega = 0)$ in terms of the retarded single particle Green's function, i.e.,

$$\chi^0(\mathbf{r}, \mathbf{r}', \omega = 0) = -2 \text{Im} \int_{-\infty}^{E_F} \frac{d\omega}{\pi} G^+(\mathbf{r}, \mathbf{r}', \omega) G^+(\mathbf{r}', \mathbf{r}, \omega). \quad (20)$$

This allows us to use our RSMS framework to calculate the response functions and thus the Hubbard interaction. Since the interactions in question are limited in spacial extent around a single atomic site, we make the approximation that the Coulomb interaction may be replaced by its spherical average about that site, i.e., $v(\mathbf{r}-\mathbf{r}') = 1/r_>$, where \mathbf{r}, \mathbf{r}' are relative to the center of the atomic site. In addition we neglect the angular momentum off-diagonal elements of the Green's function. This gives the following simple expression for the spherically averaged non-interacting response function,

$$\chi^0(r, r', \omega = 0) = -2 \text{Im} \int_{-\infty}^{E_F} \frac{d\omega}{\pi} \times \sum_L G_{LL}^+(\mathbf{r}, \mathbf{r}', \omega) G_{LL}^+(\mathbf{r}', \mathbf{r}, \omega). \quad (21)$$

We then find the RPA response function by inverting in real space. Within these same approximations, we may calculate the response function χ_r^0 defined above by omitting the angular momentum states of interest (d - or f -states) from the sum in the above equation within a cutoff radius R_c . For example to find U for the d -states, we use the response function

$$\chi_r^0(r, r', \omega = 0) = -2 \text{Im} \int_{-\infty}^{E_F} \frac{d\omega}{\pi} \times \left[\sum_{L \neq d} G_{LL}^+(\mathbf{r}, \mathbf{r}', \omega) G_{LL}^+(\mathbf{r}', \mathbf{r}, \omega) + G_{dd}^+(\mathbf{r}, \mathbf{r}', \omega) G_{dd}^+(\mathbf{r}', \mathbf{r}, \omega) \Theta(r - R_c) \Theta(r' - R_c) \right], \quad (22)$$

where $\Theta(r)$ is a smooth cutoff function which goes to zero at $r = R_c$. Finally, U is found according to Eq. (18) and (19). These RSMS calculations have been used to find the RPA screened core-hole potential in calculations of XAS, and give reasonable results when compared to other theories (i.e., final state rule or Bethe Salpeter) and experiment.³⁶ We find that a cutoff radius $R_c = 1.5R_n$ gives reasonable values of U when compared to other calculations, and consistent band gaps when compared to experiment. Fig. 1 shows a comparison of our cRPA results for U with the cRPA and cLDA results of Ref. 23. Overall, the values are in reasonable agreement, and differences can be attributed to the choice of localized states and the approximations in the treatment of screening in our method.

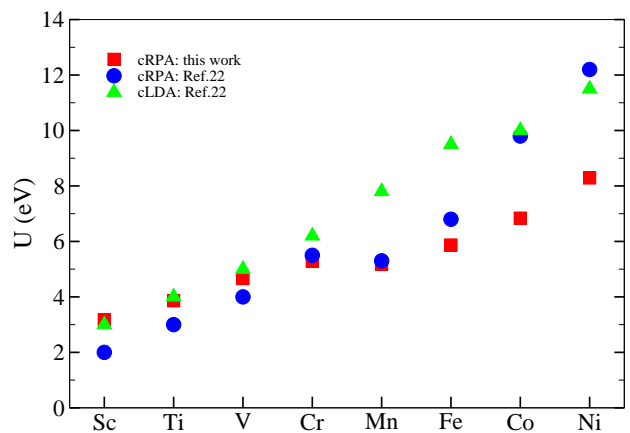


FIG. 1: (Color online) Results of our cRPA calculations of U (red squares) for the $3d$ transition metals compared with the cRPA (blue circles) and cLDA (green triangles) calculations of Aryasetiawan.²³

D. Rotationally invariant LDA+ U formalism

Our construction of $V_{lm\sigma}^U(E)$ is adapted from the LDA+ U approach of Anisimov *et al.*⁵ In their approach one starts with the total energy functional of the system and adds a Hubbard correction to account for the Coulomb interaction between localized, strongly correlated electrons. It is generally assumed³⁷ that a similar mean-field term should exist in LDA or other DFT approaches which must be subtracted from the energy functional to avoid double counting,

$$E^U[n^\sigma(\vec{r}), \mathbf{n}^\sigma] = E^{LDA}[n^\sigma(\vec{r})] + E^U[\mathbf{n}^\sigma] - E_{dc}[\mathbf{n}^\sigma], \quad (23)$$

where $n^\sigma(\vec{r})$ is the charge density, \mathbf{n}^σ the density matrix, E^U the Hubbard interaction, and E_{dc} the double

counting term. The Hubbard term depends on the density matrix $n_{ilm,ilm'}^{\sigma\sigma'}$, and on-site Coulomb interactions between the localized electrons.

For systems where the localized electrons are atomic-like, the density matrix can sometimes be approximated³⁸ as

$$n_{mm'}^{\sigma} = n_m^{\sigma} \delta_{mm'}. \quad (24)$$

This spherical approximation is often not reasonable for many systems including TMOs, and good agreement for the band gap is found only when the non-sphericity of d-d interaction as well as the off-diagonal terms of $n_{mm'}$ are taken into account.³⁸ In order to implement basis independent formalism of LDA+ U , we diagonalize the density matrix \mathbf{n}^{σ} by a unitary transformation from the $|lm\rangle$ to $|l\alpha\rangle$ basis for $3d$ states,

$$\tau * \{n_{lmm'}^{\sigma}\} * \tau^{-1} = \{n_{l\alpha}^{\sigma}\}. \quad (25)$$

The total energy functional can then be written as

$$E = E^{LDA} + \frac{1}{2} \sum_{\alpha, \alpha', \sigma} U (n_{\alpha}^{\sigma} - n^{\sigma})(n_{\alpha'}^{-\sigma} - n^{\sigma}) + \frac{1}{2} \sum_{\alpha, \alpha' \neq \alpha, \sigma} (U - J) (n_{\alpha}^{\sigma} - n^{\sigma})(n_{\alpha'}^{\sigma} - n^{\sigma}). \quad (26)$$

Here the double counting term E_{dc} is represented by n^{σ} where $n^{\sigma} = n_d/10$, and $n_d = \sum_{\alpha\sigma} n_{\alpha}^{\sigma}$. Using $V(\vec{r}) = \delta E / \delta n_{\sigma}(\vec{r})$, a simplified expression for the total LDA+ U potential is finally obtained,³⁸ i.e.,

$$V^{LDA+U}(\vec{r}) = V^{LDA}(\vec{r}) + V_{l\alpha\sigma}^U, \quad (27)$$

where

$$V_{l\alpha\sigma}^U = U \sum_{\alpha'} (n_{l\alpha'}^{-\sigma} - n^{\sigma}) + (U - J) \sum_{\alpha' \neq \alpha} (n_{l\alpha'}^{\sigma} - n^{\sigma}). \quad (28)$$

In a single-step spin-dependent calculation using the von Barth-Hedin LSDA functional, we first obtain $n_{l\alpha}^{\sigma}$. In this prescription, a prior knowledge of spin polarization of i -th atom $m_i = n_i^{\uparrow} - n_i^{\downarrow}$ is required. For Mn, Ni, and Cu we used $m = 5, 2$, and 1 respectively using Hund's multiplicity rule^{39,40} for free atoms which is often a good approximation for such systems.

The occupancy of the spin-up and -down states within the d -orbitals are thus determined in this single-step LSDA approach. Our calculations of spin-orbital occupancies of Mn and Ni d -states using this scheme are listed in Tables I and II. Thus we essentially start with a spin dependent ground state calculation and introduce spin and orbital dependence using Anisimov's prescription of Hubbard model. This LDA+ U prescription is found to provide good agreement between the theory and experiment for the XAS of the TM compounds investigated here, although the self-consistent LDA+ U treatment may be more desirable in other cases. The exchange parameter J is typically much smaller than U and variations

were found³ to be small over the transition metals; thus we have used $J=0.9$ eV for all cases. Using Eq. (12), (17), (18), and (21), we then correct our self-consistent potential and obtain a new potential $V(\mathbf{r}, E)$.

Then using the above Hubbard corrected Hamiltonian, the wave functions $R_{l\alpha}(\mathbf{r}, E)$ and $H_{l\alpha}(\mathbf{r}, E)$ are recalculated as solutions of the Schrödinger equation inside the muffin-tin spheres. The orbital dependent phase shifts $\delta_{l\alpha}^{\sigma}(E)$ are obtained by matching to the free solutions (spherical Bessel functions) at the muffin-tin, and the scattering t -matrices are found,

$$t_{l\alpha}^{\sigma} = e^{i\delta_{l\alpha}^{\sigma}} \sin(\delta_{l\alpha}^{\sigma}). \quad (29)$$

Finally the multiple-scattering equations are resolved with these t -matrices yielding the the total Green's function $G = G^c + G^{sc}$, which now includes the Hubbard- U correction. With the addition of the state dependent Hubbard correction, the potential of Eq. (12) can correctly account for the well known discontinuity^{38,41} in exact DFT exchange-correlation potentials. However, such a term is absent from the conventional LDA and GGA approaches, rendering them incapable of including such band-gap corrections.

III. RESULTS AND DISCUSSION

A. Transition Metal Oxides

Transition metal oxides (TMOs) such as MnO and NiO are considered to be prototypes of strongly correlated Mott type insulators, with localized and partially filled d -electrons at the metal sites. These TMOs have NaCl like crystal structures, (Cubic O_h^5 symmetry, and f_{m3m} space group). Below their respective Néel temperatures, they all exhibit a rhombohedral distortion due to anti-ferromagnetic (AF) ordering, which is also known as exchange anisotropy.⁴² We also examined the effects of such crystal distortions but they had negligible influence on the spectral features of interest here. In the following subsections we present results for the total and angular momentum projected DOS of MnO and NiO for a few values of U . For both compounds, the O K-edge XAS and XES are also calculated and compared with experimental results.

1. MnO

In order to compare with room temperature experiment,²⁴ we used an undistorted MnO crystal with $a = b = c = 4.4316$ Å and $\alpha = \beta = 90.624^{\circ}$.⁴³ In this paper, we do not consider periodic magnetic effects; however, the single site moments are implicitly taken into account in our $\Sigma^U(E)$ implementation. Our calculated cRPA U for MnO was found to be 5.4 eV. In our FMS RMS calculations for MnO, we used a cluster of 250

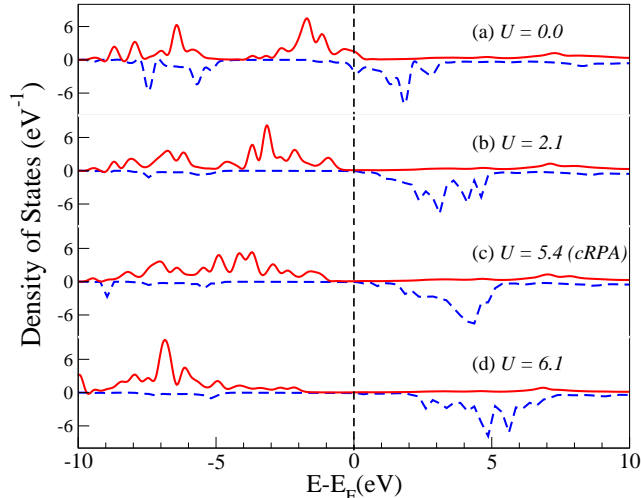


FIG. 2: (Color online) U dependence on total DOS of MnO with spin up (solid red) and spin down (dashed blue) for different values of U : (a) LDA ($U=0$), (b) $U = 2.1$ eV, (c) $U = 5.4$ eV (cRPA), and (d) $U = 6.1$ eV; the vertical dashed line is at the Fermi energy.

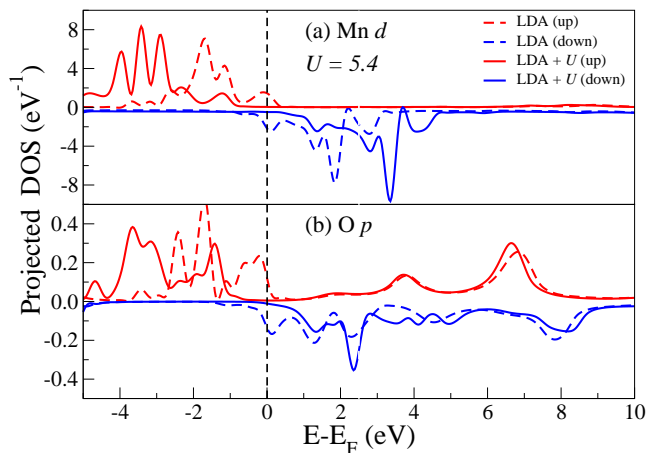


FIG. 3: (Color online) Angular momentum projected l -DOS for Mn and O in MnO with $U = 0.0$ eV (dashed lines) and cRPA $U = 5.4$ eV (solid lines); Spin up and down DOS are above and below the horizontal axis correspondingly: (a) Mn d -DOS, and (b) O p -DOS; the vertical dashed line is at the Fermi energy.

atoms, which was adequate to converge the spectrum, and a smaller cluster of 60 atoms for the self-consistent muffin-tin potentials. For this system we calculated the O K-edge XES and XAS and the spin and angular momentum projected DOS about the Mn and O sites with and without Hubbard corrections. Fig. 2 shows a comparison of our calculated total ground state spin-resolved

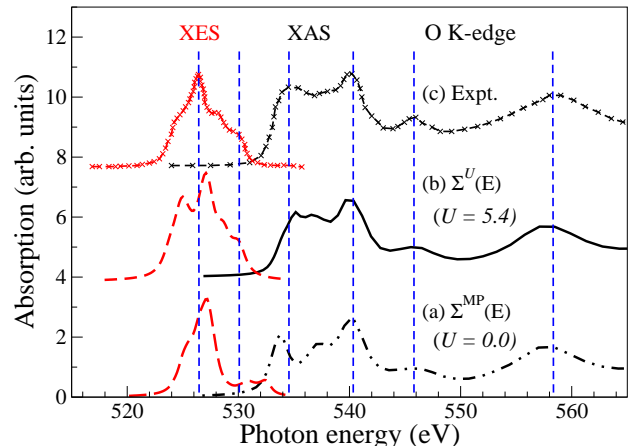


FIG. 4: (Color online) O K-edge XAS (black) and XES (red) in MnO. (a) QP FEFF calculation using our MPSE model $\Sigma^{MP}(E)$, (b) $\Sigma^U(E)$ with $U = 5.4$, and (c) experiment.²⁴ The vertical dashed lines are a guide to the eye.

DOS of MnO to that calculated with different values of U including its cRPA value. While a calculation with a MPSE underestimates an insulating gap (dashed blue line in Fig. 2), a gap close to that observed in experiment is obtained using our calculated Hubbard correction with $U = 5.4$ eV. When this Hubbard correction is applied to Mn d -states, the unoccupied spin down states are shifted by +1.6 eV, as seen in Fig. 3(a). The O p -states (Fig. 3(b)) near E_F are strongly hybridized with Mn d -states (Fig. 3(a)); thus a gap is also seen in the O p -DOS. However, the O p -states around 6-8 eV only hybridize with Mn s - p -states (not shown) and are not affected by the Hubbard correction. In Table (I) we present the spin-orbital occupancies of the localized Mn d -states and the corresponding Hubbard correction for $U = 5.4$ and $J = 0.9$ eV.

TABLE I: Mn d -state parameters ($U = 5.4$ eV; $J = 0.9$ eV)

l	α	$n_{l\alpha}$	$n_{l\alpha}^\uparrow$	$n_{l\alpha}^\downarrow$	$V_{l\alpha}^\uparrow$ (eV)	$V_{l\alpha}^\downarrow$ (eV)
2	α_1	0.94	0.85	0.09	-0.32	3.11
2	α_2	0.90	0.81	0.09	-0.29	3.11
2	α_3	0.93	0.83	0.10	-0.30	3.12
2	α_4	1.10	0.99	0.11	-1.00	3.12
2	α_5	1.09	0.98	0.11	-1.00	3.15

Bulk sensitive XES and XAS for TM oxides often provide a good assessment of the band gap in insulators.²⁴ In Fig. 4 we compare our Σ^U calculation of the O K-edge XAS and XES with experiment.²⁴ Fig. 4 shows the result of our spin resolved FMS calculation obtained with both Hubbard and MPSE corrections (b), compared to results with no Hubbard correction (a), and experiment

(c). The XAS calculation was done in the presence of a screened core-hole at the absorbing O atom while for XES no core-hole was included; these approximations are consistent with the final-state- and initial-state rules for XAS and XES respectively. Our Hubbard corrected self-energy blue shifts the first excitation at around 534 eV, while the rest of the unoccupied states, including the main peak at 540 eV, are unchanged. In XES, the highest occupied state moves down by 3 eV which is now on the other side of the second vertical dashed line in Fig. 4. These distinct, opposite shifts of the highest occupied and first unoccupied states are due to the strong hybridization of O p -states with the localized Mn d states. This can also be identified in Fig. 3(b) as the lower (LHB) and upper Hubbard bands (UHB) at around -2 and 2 eV.

2. NiO

In order to compare with room-temperature experiments²⁴ we have accounted for the rhombohedral distortion of NiO crystal along the [111] direction.^{44,45} Our methods for calculating electronic structures of NiO are similar to those for MnO, except for the input NiO crystal structure, where we have used a slightly distorted crystal with $a = b = 4.168$ Å, $c = 4.166$ Å, and $\alpha = \beta = 90.055^\circ$, $\gamma = 90.082^\circ$. With the Hubbard correction, the best agreement with the experimental XAS was again obtained with our calculated $U = 8.0$ eV. Fig. 5 shows the gap opening in the spin projected total DOS of NiO for other values of U beside cRPA U . The O p -states in NiO are also strongly hybridized

TABLE II: Ni d -state parameters ($U = 8.0$ eV; $J = 0.9$ eV)

l	α	$n_{l\alpha}$	$n_{l\alpha}^\uparrow$	$n_{l\alpha}^\downarrow$	$V_{l\alpha}^\uparrow$ (eV)	$V_{l\alpha}^\downarrow$ (eV)
2	α_1	1.21	0.91	0.30	-0.72	3.95
2	α_2	1.30	0.95	0.35	-1.40	4.02
2	α_3	1.86	0.95	0.91	-1.40	-0.52
2	α_4	1.86	0.95	0.91	-1.40	-0.52
2	α_5	1.88	0.96	0.92	-1.43	-0.53

with localized Ni d -states as in MnO. The spin-orbital occupancies and corresponding Hubbard potential for the Ni d -states are listed in Table II.

Our GW plasmon-pole calculation in Fig. 7(a) exhibits considerable overlap between the O K-edge XAS and XES spectra, due to the underestimated insulating gap. However, the introduction of the Hubbard interaction ($U = 8.0$ eV) increases the gap, causing the pre-peaks of both the XAS and XES to split further apart, as shown in Fig. 7(c). For comparison, we also show a WIEN2K LDA+ U calculation in Fig. 7(a) for the O K-edge EELS in NiO.⁴⁶

Aligning the first peak of this calculation with experiment [Fig. 7(d)], we observe an underestimation of the high energy peaks at around 544 eV. These peaks

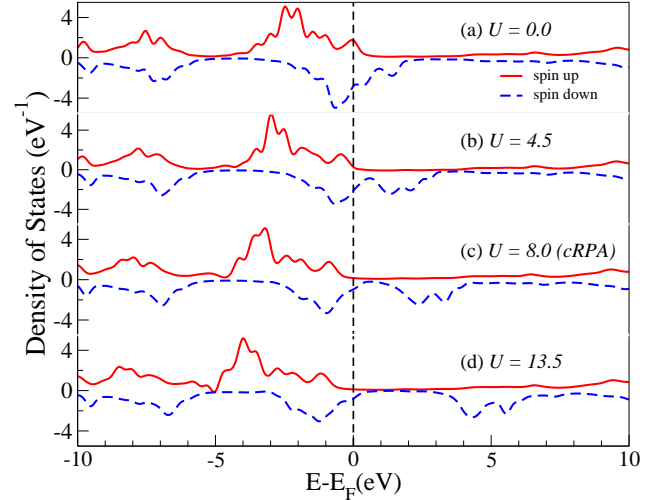


FIG. 5: (Color online) U dependence on total DOS of NiO with spin up (solid red) and spin down (dashed blue) for different values of U : (a) $U = 0$ eV, (b) $U = 4.5$ eV, (c) $U = 8.0$ eV (cRPA), and (d) $U = 13.5$ eV; the vertical dashed line is at the Fermi energy.

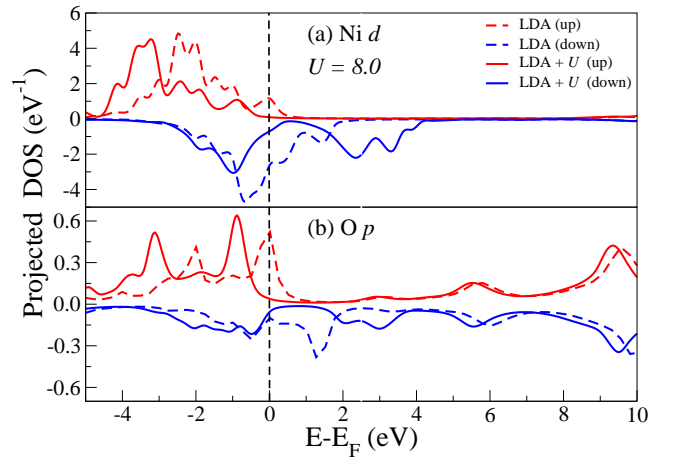


FIG. 6: (Color online) angular momentum projected l -DOS for Ni and O in NiO with $U = 0.0$ eV (dashed line), and $U = 8.0$ eV (solid line); Spin up and down DOS are above and below the horizontal axis correspondingly: (a) Ni d -DOS (b) O p -DOS; the vertical dashed line is at the Fermi energy.

can be attributed to O p -states which are strongly hybridized with Ni s - and p -states. Similar behavior has been found in NiO,^{6,47} and other TM compounds.^{46,48} We attempted to improve these results by using a GW MPSE³³ for NiO, while applying the Hubbard correction to the Ni d -states. This MPSE model includes a more realistic treatment of inelastic losses than the plasmon pole model, and yields improved agreement with exper-

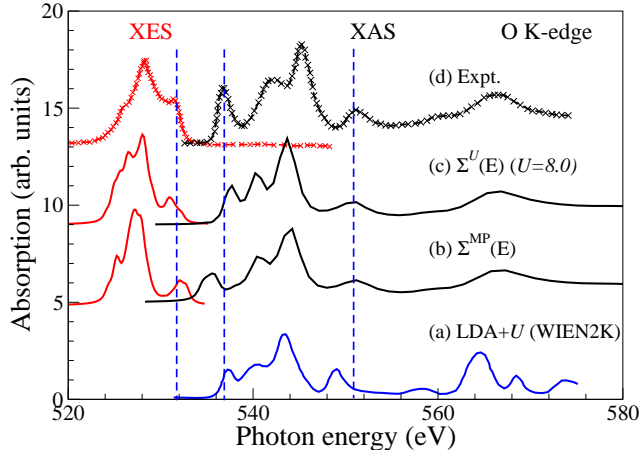


FIG. 7: (Color online) NiO O K-edge XAS (black) and XES (red) experiment vs theory: (a) LDA+ U calculation⁴⁶ for O 1s EELS using WIEN2K; (b) FEFF GW plasmon-pole (PP) self-energy; (c) FEFF $\Sigma^U(E)$ with *ab initio* Hubbard correction with cRPA $U = 8.0$ eV; and (d) Experiment.²⁴ The vertical dashed lines are a guide to the eye.

iment, as seen in Fig. 7(c). These results demonstrate that an accurate treatment of the delocalized s - p -states can also be important in such systems. Thus in order to achieve good agreement between theoretical and experimental spectral features, a systematic consideration of excited state properties including both localized- and delocalized states is important.

TABLE III: Calculated Hubbard parameter U and gap Δ of MnO, NiO, and LSCO.

Materials	MnO	NiO	LSCO
U (this work)	5.4	8.0	10.0
U (Ref. 6)	4.7	5.2	
U (Ref. 3)	6.9	8.0	
Δ (this work)	3.9	4.4	1.4
Δ (Ref. 6)	2.6	3.8	
Δ (Expt. ^{24,49})	4.1	4.3	1.8

In Table III we compare our cRPA calculated U and estimated XAS-XES gap Δ with gap values reported by others. Our values of U for MnO and NiO are in reasonable accord with experiment and roughly comparable to those of Ref. 3,6. Likewise our calculated values of Δ are in good agreement with experiment for MnO and NiO, but underestimated by 0.5 eV for LSCO. We have also compared in Fig. 8 our total DOS for MnO calculated with our cRPA $U = 5.4$ and $J = 0.9$ eV, with that of Ref. 6 calculated with $U = 5.4$ and $J = 0.0$. Despite differences in methodology and the fact that the gap Δ can

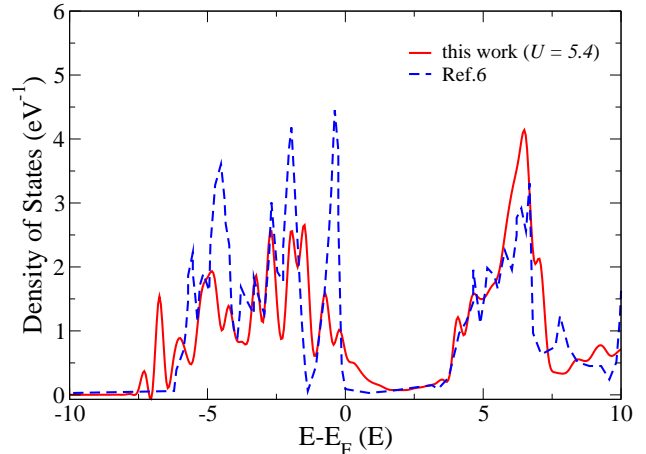


FIG. 8: (Color online) MnO total DOS with our RSMS cRPA calculated $U = 5.4$ and $J = 0.9$, and GW@LDA+ U calculations⁶ with $U = 5.4$ $J = 0.0$ (dashed blue line); the vertical dashed line is at the Fermi energy.

only be determined approximately with a finite cluster RSMS approach, both methods are in reasonable agreement.

B. LSCO

Understanding the doping dependence of high T_c cuprates has become an interesting challenge in recent years. LSCO ($\text{La}_{2-x}\text{Sr}_x\text{CuO}_4$), which is a prototype of hole-doped cuprates, exhibits metallic and paramagnetic behavior at high doping,¹¹ and becomes an AF insulator when undoped. Between these limits, the system goes through a superconducting phase at the doping concentration of about $x = 0.15$. A good description of the electronic structure in its insulating phase is important to understand the exotic doping dependent phase transformations in such systems.

In the over-doped region with $x > 0.2$, LSCO becomes paramagnetic, and is well described by a self-energy approximation constructed from a single band Hubbard model.¹¹ A Fermi-liquid description thus becomes more appropriate for such systems. As doping is reduced, correlation effects due to localized states become more important, and the implementation of Hubbard U to the d electrons on the Cu sites is seen to open a gap. A gap correction using $\Sigma^U(E)$ on the partial d -DOS of Cu and p -DOS of O is shown in Fig. 9. Our O K-edge XAS for $\Sigma^{MP}(E)$ and Σ^U with $U = 10.0$ eV are compared with experimental results in Fig. 11. Our result with cRPA calculated U agrees well with the undoped LSCO experiment, while the over-doped LSCO system is reasonably reproduced by a GW MPSE calculation alone ($U = 0$).

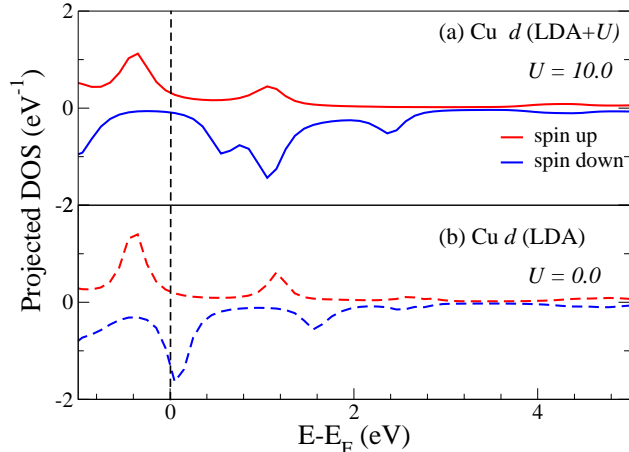


FIG. 9: (Color online) (a) Cu spin up (solid red) and down (solid blue) d -DOS of LSCO with cRPA calculated value $U = 10.0$; (b) Cu spin up and down d -DOS for $U = 0.0$ (dashed red and blue). The vertical dashed line is at the Fermi energy.

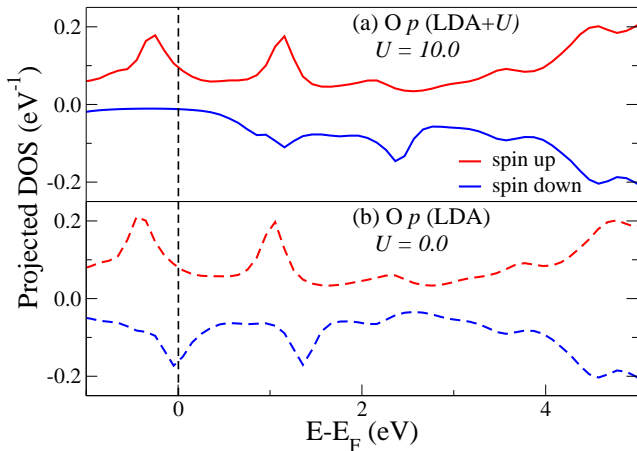


FIG. 10: (Color online) (a) O spin up (solid red) and down (solid blue) p -DOS of LSCO with cRPA $U = 10.0$; (b) O spin up (dashed red) and down (dashed blue) p -DOS with $U = 0.0$. The vertical dashed line is at the Fermi energy.

This result is not surprising, since in the absence of the Hubbard term, the LDA does not predict a correlation gap. As a result the system is predicted to be metallic, mimicking the over-doped ($x \approx 0.3$) paramagnetic phase of $\text{La}_{1-x}\text{Sr}_x\text{CuO}_4$. A complete description of the doping dependence of spectral features from over-doped ($x = 0.3$) to undoped ($x = 0.0$), requires a dynamical self-energy correction that incorporates pseudo-gap, superconducting, and Fermi-liquid physics.⁵⁰

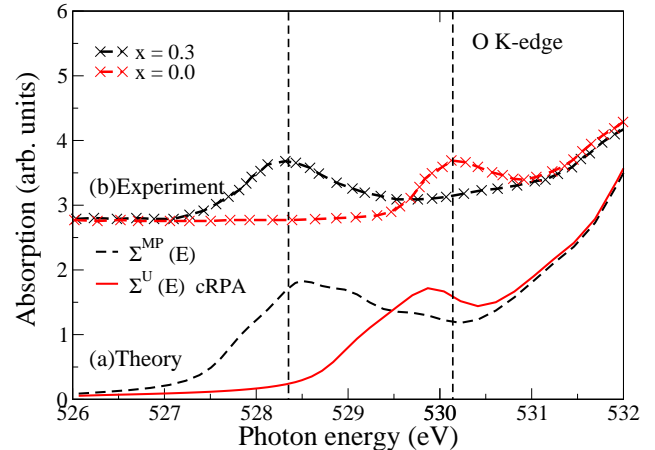


FIG. 11: (Color online) O K-edge XAS for LSCO: (a) our $\Sigma^U(E)$ calculation with cRPA $U = 10.0$ (red) and GW only (black); (b) experimental K-edge XAS for undoped ($x = 0.0$, red) and over-doped ($x = 0.3$, black) LSCO, and the vertical dashed lines are a guide to the eye.

IV. SUMMARY AND CONCLUSIONS

We have implemented Hubbard model corrections within an LDA+ U approach, using a rotationally invariant formalism and an extension of the RSMS Green's function method for calculations of excited state electronic structure and x-ray spectra of correlated materials. Our approach also builds in a model GW self-energy. Both Hubbard-model and dynamic self-energy effects are incorporated in an effective self-energy correction $\Delta\Sigma^U$. The Hubbard parameter U is estimated using the cRPA method, again within the RSMS formalism. The additional GW self-energy is approximated by a many-pole model based on the electron gas Green's function and the loss function in the long-wavelength limit. These considerations lead to a RSMS/ $\Delta\Sigma^U$ approach which provides an efficient way to account for correlation effects on x-ray spectra of complex materials. The approach is advantageous for aperiodic systems since it does not rely on symmetry or periodicity. The method was tested on several correlated materials and found to yield reasonable agreement for the observed experimental band gap as well as the XAS and XES of MnO and NiO. However, the agreement with experiment is less accurate for more complex systems such as LSCO. This suggests the need in such systems for a more comprehensive treatment of superconducting and pseudo-gap physics that incorporates doping dependence in the under-doped regime.^{8,50} Overall, however, our method explains the key features of the excited state electronic structure and spectra of

many strongly correlated systems, and in particular the correlation gap. Finally we note that our approach is limited to the quasi-particle approximation and Hubbard model corrections, while inelastic many-body effects such as satellites and charge-transfer excitations are currently neglected.

V. ACKNOWLEDGMENT

We thank A. Bansil and R. Markiewicz, and especially P. Rinke for stimulating suggestions. This work is supported by the Division of Materials Science & Engineering, Basic Energy Sciences, US Department of Energy Grants DE-FG03-97ER45623 and DE-FG02-07ER46352. This research also benefited from the collaboration supported by the Computational Materials Science Network (CMSN) program of US DOE under grant DE-FG02-08ER46540.

-
- ¹ G. Onida, L. Reining, and A. Rubio, *Rev. Mod. Phys.* **74**, 601 (2002).
- ² L. Hedin and S. Lundqvist, *Solid State Phys.* **23**, 1 (1969).
- ³ V. I. Anisimov, J. Zaanen, and O. K. Andersen, *Phys. Rev. B* **44**, 943 (1991).
- ⁴ A. I. Liechtenstein, V. I. Anisimov, and J. Zaanen, *Phys. Rev. B* **52**, R5467 (1995).
- ⁵ V. I. Anisimov, F. Aryasetiawan, and A. I. Liechtenstein, *J. Phys.: Condens. Matter* **9**, 767 (1997).
- ⁶ H. Jiang, R. I. Gomez-Abal, P. Rinke, and M. Scheffler, *Phys. Rev. B* **82**, 045108 (2010).
- ⁷ H. Jiang, R. I. Gomez-Abal, P. Rinke, and M. Scheffler, *Phys. Rev. Lett.* **102**, 126403 (2009).
- ⁸ T. Das, R. S. Markiewicz, and A. Bansil, *Phys. Rev. B* **81**, 174504 (2010).
- ⁹ R. S. Markiewicz, S. Sahrakorpi, and A. Bansil, *Phys. Rev. B* **76**, 174514 (2007).
- ¹⁰ S. Basak, T. Das, H. Lin, J. Nieminen, M. Lindroos, R. S. Markiewicz, and A. Bansil, *Phys. Rev. B* **80**, 214520 (2009).
- ¹¹ T. Ahmed, T. Das, J. J. Kas, H. Lin, B. Barbiellini, F. D. Vila, R. S. Markiewicz, A. Bansil, and J. J. Rehr, *Phys. Rev. B* **83**, 115117 (2011).
- ¹² O. Bengone, M. Alouani, P. Blöchl, and J. Hugel, *Phys. Rev. B* **62**, 16392 (2000).
- ¹³ H. Ebert, A. Perlov, and S. Mankovsky, *Solid State Communications* **127**, 443 (2003).
- ¹⁴ A. Juhin, F. de Groot, G. Vankó, M. Calandra, and C. Brouder, *prb* **81**, 115115 (2010).
- ¹⁵ O. Gunnarsson, *Phys. Rev. B* **41**, 514 (1990).
- ¹⁶ A. K. McMahan, R. M. Martin, and S. Satpathy, *Phys. Rev. B* **38**, 6650 (1988).
- ¹⁷ M. S. Hybertsen, M. Schlüter, and N. E. Christensen, *Phys. Rev. B* **39**, 9028 (1989).
- ¹⁸ I. V. Solovyev and M. Imada, *Phys. Rev. B* **71**, 045103 (2005).
- ¹⁹ M. Cococcioni and S. de Gironcoli, *Phys. Rev. B* **71**, 035105 (2005).
- ²⁰ K. Nakamura, R. Arita, Y. Yoshimoto, and S. Tsuneyuki, *Phys. Rev. B* **74**, 235113 (2006).
- ²¹ M. Springer and F. Aryasetiawan, *Phys. Rev. B* **57**, 4364 (1998).
- ²² F. Aryasetiawan, M. Imada, A. Georges, G. Kotliar, S. Biermann, and A. I. Liechtenstein, *Phys. Rev. B* **70**, 195104 (2004).
- ²³ F. Aryasetiawan, K. Karlsson, O. Jepsen, and U. Schönberger, *Phys. Rev. B* **74**, 125106 (2006).
- ²⁴ E. Z. Kurmaev, R. G. Wilks, A. Moewes, L. D. Finkelstein, S. N. Shamin, and J. Kuneš, *Phys. Rev. B* **77**, 165127 (2008).
- ²⁵ P. Krüger, *Journal of Physics: Conference Series* **190**, 012006 (2009).
- ²⁶ J. J. Rehr, J. J. Kas, F. D. Vila, M. P. Prange, and K. Jorissen, *Phys. Chem. Chem. Phys.* **12**, 5503 (2010).
- ²⁷ J. J. Rehr, J. J. Kas, M. P. Prange, A. P. Sorini, Y. Takimoto, and F. Vila, *Comptes Rendus Physique* **10**, 548 (2009).
- ²⁸ A.L. Ankudinov and J.J. Rehr, *Phys. Rev. B* **62**, 2437 (2000).
- ²⁹ U. von Barth and L. Hedin, *J. Phys. C: Solid State Phys.* **5**, 1629 (1972).
- ³⁰ A.L. Ankudinov, B. Ravel, J.J. Rehr, , and S.D. Conradson, *Phys. Rev. B* **58**, 7565 (1998).
- ³¹ J. J. Rehr and R. C. Albers, *Rev. Mod. Phys.* **72**, 621 (2000).
- ³² W. von der Linden and P. Horsch, *Phys. Rev. B* **37**, 8351 (1988).
- ³³ J. J. Kas, A. P. Sorini, M. P. Prange, L. W. Cambell, J. A. Soininen, and J. J. Rehr, *Phys. Rev. B* **76**, 195116 (pages 10) (2007).
- ³⁴ A. Georges, *AIP Conference Proceedings* **715**, 3 (2004).
- ³⁵ M. J. Stott and E. Zaremba, *Phys. Rev. A* **21**, 12 (1980).
- ³⁶ A. L. Ankudinov, Y. Takimoto, and J. J. Rehr, *prb* **71**, 165110 (2005).
- ³⁷ R. C. Albers, N. E. Christensen, and A. Svane, *J. Phys.: Condens. Matter* **21**, 343201 (2009).
- ³⁸ V. I. Anisimov, I. V. Solovyev, M. A. Korotin, M. T. Czyżyk, and G. A. Sawatzky, *Phys. Rev. B* **48**, 16929 (1993).
- ³⁹ B. Fromme, *Electronic Structure of MnO, CoO, and NiO*, vol. 170 of *Springer Tracts in Modern Physics* (Springer Berlin Heidelberg, 2001).
- ⁴⁰ S. Liu and W. Langenaeker, *Theoretical Chemistry Accounts: Theory, Computation, and Modeling (Theoretica Chimica Acta)* **110**, 338 (2003).
- ⁴¹ J. P. Perdew, R. G. Parr, M. Levy, and J. L. Balduz, *Phys. Rev. Lett.* **49**, 1691 (1982).
- ⁴² A. E. Berkowitz and K. Takano, *Journal of Magnetism and Magnetic Materials* **200**, 552 (1999).
- ⁴³ B. Morosin, *Phys. Rev. B* **1**, 236 (1970).
- ⁴⁴ K. Nakahigashi, N. Fukuoka, and Y. Shimomura, *J. Phys. Soc. Jpn.* **38**, 1634 (1975).
- ⁴⁵ H. Kondoh and T. Takeda, *J. Phys. Soc. Jpn.* **19**, 2041 (1964).
- ⁴⁶ L. V. Dobysheva, P. L. Potapov, and D. Schryvers, *Phys. Rev. B* **69**, 184404 (2004).
- ⁴⁷ H. Kurata, E. Lefèvre, C. Colliex, and R. Brydson, *Phys. Rev. B* **47**, 13763 (1993).
- ⁴⁸ T. Kotani and M. van Schilfgaarde, *J. Phys.: Condens. Matter* **20**, 295214 (2008).
- ⁴⁹ J. Orenstein, G. A. Thomas, D. H. Rapkine, C. G. Bethea, B. F. Levine, R. J. Cava, E. A. Rietman, and D. W. Johnson, *Phys. Rev. B* **36**, 729 (1987).
- ⁵⁰ R. S. Markiewicz, T. Das, and A. Bansil, *Phys. Rev. B* **82**, 224501 (2010).